How to cite: *Angew. Chem. Int. Ed.* **2024**, *63*, e202316696
doi.org/10.1002/anie.202316696

Helical Structures

Can Magnetic Dipole Transition Moment Be Engineered?

Rafael G. Uceda[+], Carlos M. Cruz[+], Sandra Míguez-Lago, Luis Álvarez de Cienfuegos, Giovanna Longhi, David A. Pelta, Pavel Novoa, Antonio J. Mota,* Juan M. Cuerva,* and Delia Miguel**

Abstract: The development of chiral compounds with enhanced chiroptical properties is an important challenge to improve device applications. To that end, an optimization of the electric and magnetic dipole transition moments of the molecule is necessary. Nevertheless, the relationship between chemical structure and such quantum mechanical properties is not always clear. That is the case of magnetic dipole transition moment (***m***) for which no general trends for its optimization have been suggested. In this work we propose a general rationalization for improving the magnitude of ***m*** in different families of chiral compounds. Performing a clustering analysis of hundreds of transitions, we have been able to identify a single group in which $|m|$ value is maximized along the helix axis. More interestingly, we have found an accurate linear relationship (up to $R^2 = 0.994$) between the maximum value of this parameter and the area of the inner cavity of the helix, thus resembling classical behavior of solenoids. This research provides a tool for the rationalized synthesis of compounds with improved chiroptical responses.

Introduction

Since the discovery of optical activity in the nineteenth century, much effort has been made to understand the chiroptical phenomena. The use of such knowledge as a tool to create entities with magnified chiroptical responses implies a step forward. Such chiroptical properties have been suggested to be relevant in many areas,[1] such as 3D displays,[2] optoelectronic devices,[3–5] chiral sensing,[6] optical switches[7–9] and, also, in physical phenomena as the chiral induced spin selectivity (CISS) effect,[10–14] with applications in spin-selective electrochemical and biological processes.[15,16]

Among the chiroptical properties, electronic circular dichroism (ECD) has dominated the field owing to the well-established equipment for its measurement, and the relevant structural information that provides. The main drawback is the usually weak signal associated to this property. The magnitude of the response for each transition depends on a critical parameter, the rotatory strength (R), which is related to the scalar product of the electric (μ) and magnetic (m) dipole transition moments, $\boldsymbol{\mu}\cdot\boldsymbol{m} = |\mu|\cdot|m|\cdot\cos\theta$, being $|\mu|$ and $|m|$ the corresponding modules and θ the angle between the two vectors. The disparity in the magnitude of both dipole moments and the misalignment between them is at the core of the problem. For an ideal intense response, both dipoles should be aligned, being also both as high in magnitude as possible. Although μ can be engineered promoting a displacement of charge during the transition, there is no clear idea on how to enhance m. It is worth noting that one of the most challenging facts in ECD is that high absorption dissymmetry factors ($g_{abs} = \Delta\varepsilon/\varepsilon \approx 4(|m|/|\mu|)\cos\theta$) are often associated with low absorption values, that is low μ (a typical example is the electric dipole forbidden transition of carbonyl). For a related phenomenon as circularly polarized luminescence (CPL) the desired high emission dissymmetry factor for the $S_1 \rightarrow S_0$ transition ($g_{lum} = \Delta I/I \approx 4(|m|/|\mu|)\cos\theta$), is also incompatible with high quantum yields by a similar reasoning.[17] A rough estimation

[*] R. G. Uceda,[+] Dr. C. M. Cruz,[+] Dr. S. Míguez-Lago, Prof. L. Á. de Cienfuegos, Prof. J. M. Cuerva
Departamento de Química Orgánica, Unidad de Excelencia de Química Aplicada a la Biomedicina y Medioambiente (UEQ), Universidad de Granada (UGR), Facultad de Ciencias
C. U. Fuentenueva 18071 Granada (Spain)
E-mail: jmcuerva@ugr.es

Prof. G. Longhi
Dipartimento di Medicina Molecolare e Traslazionale, Università di Brescia
Viale Europa 11, 25123 Brescia (Italy)

Prof. D. A. Pelta, Dr. P. Novoa
Departamento de Ciencias de la Computación e Inteligencia Artificial, UGR
C/Periodista Daniel Saucedo Aranda S/N, 18071 Granada (Spain)
E-mail: pavelnovoa@ugr.es

Dr. A. J. Mota
Departamento de Química Inorgánica, UEQ, UGR, Facultad de Ciencias
C. U. Fuentenueva 18071 Granada (Spain)
E-mail: mota@ugr.es

Dr. D. Miguel
Departamento de Fisicoquímica, UEQ, UGR, Facultad de Farmacia
Avda. Profesor Clavera S/N 18071 Granada (Spain)
E-mail: dmalvarez@ugr.es

[+] These authors contributed equally to this work.

of the maximum g values for electric allowed transitions in organic molecules, considering Bohr magneton and electronic charge multiplied Bohr radius values, suggests that they are limited by twice the dimensionless fine structure constant α (rough 10^{-2}).[18] Nevertheless, the above mentioned dichotomy can change creating systems with acceptable electric- and magnetic-allowed transitions at the same time. That is, transitions with exceptional m values, while μ remains high.

Playing with the naïve idea that transitions in fully conjugated helical molecules resemble the behavior of a nanosolenoid with one or multiple loops, we could consider that electron movement during the transition develops an $\boldsymbol{m}$ whose magnitude classically depends on the area encircled by each loop (Figure 1). This reasoning recalls the "free electron on a helix" model by Tinoco and Woody, adopted in the sixties to explain optical rotation of helices.[19] If this hypothesis is correct, a linear dependence between $\boldsymbol{m}$ and the inner area within a family of nanosolenoids should exist. In that way, $\boldsymbol{m}$ could be engineered for a selected transition, in principle, with no limits. This suggestive idea is supported by previous observations of our group[20] and strengthened by the observations of a similar behavior in other helical structures by Matsuda, Don Tilley, Isobe, Wu and Itami groups.[21–26]

Herein, we have analyzed such appealing possibility in three different families of organic helical structures (simple carbo[n]helicenes and *ortho*-oligophenylethynylenes, *o*-OPEs) and a chiral molecular circuit based on paraphenylethynylene-linked paracyclophanes recently reported by Morisaki.[27] First, we need to identify the best transitions in terms of $|m|$ for each compound. If the assumption is right, the corresponding vectors should be aligned with the helix axis, as the classical viewpoint demands. The selection of transitions has been done with machine learning approach. Specifically, we chose clustering procedures that has been successfully applied in several context, including chemistry.[28] Indeed, clustering has been recently applied to tackle conformational uncertainties in chiroptical properties.[29] From the perspective of machine learning,[30] clustering is an unsupervised approach involving several methods aimed to identify groups of objects based on some measure of similarity among them.[31] In this work we relied on a clustering method on all calculated electronic transitions (100 in most cases) for each molecule in every family to determine meaningful groups of magnetic transitions. An online implementation of the code used for the clustering can be accessed at GitHub (see SI). We have found by means of density functional theory (DFT) calculations that exceptional $|m|$ values could be obtained once the orbitals involved in the transition are fully delocalized in the helix, allowing a formal helical movement of an electron along the helix axis. It is interesting to recall that in C_2-symmetric species, transitions oriented parallel to the helical axis, or with a component along the helix axis, are always of symmetry species B. Additionally, we have found that $|m|$ depends directly on the number of turns and, therefore, on the total encircled area of the solenoids. Thus, we have shown that this dependence exists and can be predicted. As a consequence of our findings, exceptional chiroptical responses can be designed and predicted with $|m|$ values up to 47×10^{-20} erg G^{-1}.

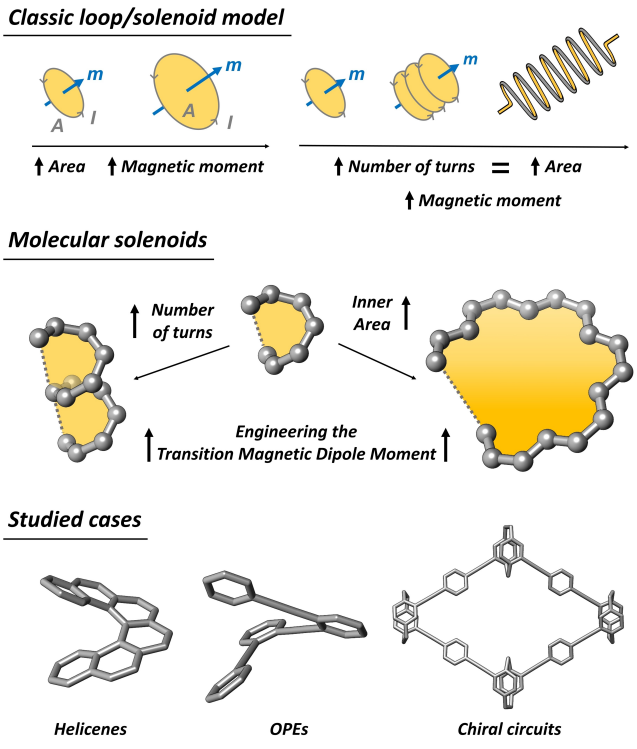

Figure 1. Summary of the theoretical model (top), strategies on how to increase the inner area (middle) and chiral families studied (bottom).

Results and Discussion

Three families of fully π-conjugated helical molecules, ranging from simple [n]helicenes to larger extended *o*-oligo(phenylene)ethynylenes (OPEs), and molecular circuits based on chiral cyclophanes[27] were studied. Within the same family, the inner area was increased in two different ways: i) increasing the number of turns and/or ii) elongating the side of the geometric form. The geometries of each member were optimized using DFT methods as implemented in Gaussian 09[32] at the LC-ωPBE[33]/6-31G*[34]/PCM[35] level of theory. Subsequently, vertical electronic transitions were computed by time dependent density functional theory (TD-DFT) at the same level of theory, and the module of $\boldsymbol{m}$ ($|m|$) calculated. To avoid any functional dependence of the present results, other functionals have been tested (B3LYP,[36–38] M06 and M06-2X)[39] (ESI). The calculated $|m|$ values for all transitions were subsequently grouped in families using an unsupervised clustering process under a statistically optimized number of subgroups. This way, no presumption is made, and a set of data can be obtained and correlated with different magnitudes. Among the several methods/algorithms available,[30] as an initial approach, we applied the k-means algorithm,[40] which produces k groups from the available data. Such algorithm

was chosen given its suitability to deal with numerical features, the low complexity of the output and the wide availability of software implementations that makes its application easy.[30] In particular, the Euclidean distance was used as a measure of similarity between objects, while the value of k (optimal number of clusters) was determined automatically from the *elbow* method.[40] In this procedure, the algorithm was applied for $k \in [2, 3, .., 20]$ and the k value that maximizes the curvature of an interpolated function of the inertia cost was kept.[41] The k-means implementation provided in the Python module scikit-*learn*[42] was used for the experiments. Remarkably, for all the studied compounds (nearly 70), there is one family, composed by one to a few components in the group, in which the vector is pointing in the helix axis with a very high relative $|m|$, as demonstrated by previous studies.[20] To our delight, we found the expected correlation: the representation of $|m|$ against the area for all the families showed an intriguing linear relationship with R^2 up to 0.994. In this way, predictive extrapolations about maximum values of $|m|$ could be made within the families. It is worth noting that for organic molecules very good values for $|m|$ are around 1×10^{-20} erg G^{-1}. In the studied series, there are transitions behaving as classical solenoids in which this value could be increased in orders of magnitude simply by varying the area. On the other hand, the existence of such transitions with a solenoid type behavior is interesting for electron transport properties through the molecule. It has been suggested that chiral systems with intense chiroptical properties are also relevant for the so called CISS effect.[12,13]

As the simplest case, we started our study with [n]helicenes. This family of *o*-fused benzenes generates well defined helical structures, being configurationally stable from [6]helicene, although [5]helicene can be isolated in an enantiopure way and characterized before its racemization.[43] Bearing this idea in mind, we calculated the vertical electronic transitions of all helicenes from [5]helicene to [30]helicene, along with [40]helicene and [50]helicene. For the first series, 100 transitions were computed, whilst for the two largest members, [40]helicene and [50]helicene, only 30 transitions were calculated due to the elevated computational cost. The clustering process was statistically optimized, yielding 6–9 subgroups. Remarkably, one of the subgroups was constituted by a unique transition with maximum $|m|$ and parallel to the helix axis (Figure 2). The exception was [9]helicene, where two transitions close in energy seemed to share the weight of the rotational strength. However, increasing the number of cluster subgroups resulted in the same observation: the initial group of maximum $|m|$ with two elements develops into a unique transition with the vector aligned with the helix axis.

To answer the question of whether the intense transitions aligned with the helix axis behaved as a classical solenoid, the $|m|$ values against the inner area of the helicene were represented (Figure 3). For the exception ([9]helicene), the maximum value of both transitions was used in the correlation (although the use of the centroid gave similar results, see SI). An impressive linear correlation was found, which fits the expected behavior from [5] to

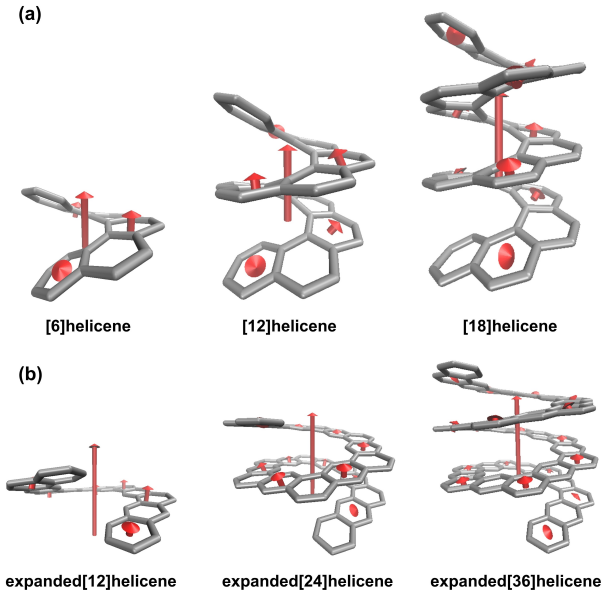

Figure 2. Optimized structures (LC-ωPBE/6-31G*/PCM) of **[6]**, **[12]** and **[18]helicene** (a) and of **expanded[12]**, **[24]** and **[36]helicene** (b) including the decomposition analyses (see SI) of the magnetic dipole transition moment (m) for the transition that represents a single independent subgroup in the cluster analysis.

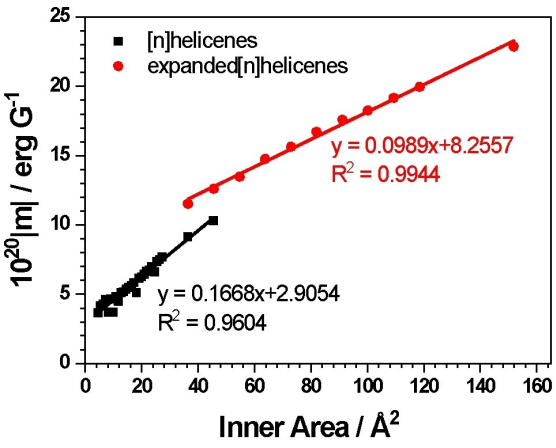

Figure 3. Correlation chart between the inner area and the calculated magnetic dipole transition moment module ($|m|$) for **[n]helicenes** (black squares) and **expanded[n]helicenes** (red circles).

[50]helicene. Apparently, no limit for $|m|$ value can be inferred from the data, the higher the area, the higher the value. It is worth noting that the optimization of this $|m|$ value would allow obtaining giant chiroptical responses owing to electric and magnetic allowed transition. This fact can be observed in the [n]helicene family, enhancing the expected value of R from 924.9 to 8378.5×10^{-40} erg esu cm G^{-1} (for [6] and [50]helicene, respectively) and, in consequence, the ECD response (Figure 4).

Magnetic dipole transition moment ***m*** could be visualized using a breakdown analysis of the densities, as implemented in the Multiwfn package.[44] As expected for the transitions chosen by clustering analysis, the ***m*** density

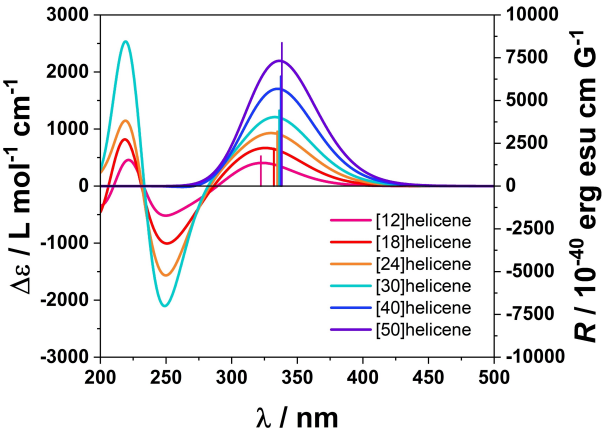

Figure 4. Simulated ECD spectra (lines) of **[12]**, **[18]**, **[24]**, **[30]**, **[40]** and **[50]helicene** (sigma = 0.40 eV) and rotatory strengths (bars) of the transition that forms a cluster itself (***m*** aligned with the helix axis).

was clearly localized around the helix, being maxima in the central part of the helix axis (Figure 5). The trend was observed from [5] to [50]helicene (see SI). Interestingly, the decomposition of ***m*** associated to the phenyl ring contributions (Figure 2) supported this observation.

After analysis of [n]helicenes, as mentioned above, another strategy to increase the inner area is to expand the side of the geometric form. Therefore, *cata*-fused helicenes (expanded helicenes) were selected as [n]helicene analogues with an increased inner area. These compounds have been proposed as an alternative to generate intense chiroptical properties and its synthesis is attracting major attention.[45–48] Within this family, we have considered examples ranging from $n = 12$ to 39 benzene rings, both included, along with $n = 50$. In this case, each loop represents a six-fold larger area than in [n]helicenes. Thus, the expanded[12]helicene represents a single turn, and the expanded[30]helicene 2.5 turns (Figure S78). This fact allowed us to preserve the number of involved benzene rings and number of turns, to perform a comparison with the previous family. Clustering process resulted in a subgroup of transitions composed by only one vector aligned with the helix axis. Not surprisingly, the magnitude of such vector correlated with the inner area along the family with an almost perfect linear relationship (Figure 3, red circles). Remarkably, the slope was similar to the one obtained for the [n]helicenes family. Even more important is the fact that the new helical arrangement was able to enclose bigger areas for the same number of benzene rings. That is, the area of the first member of the series (expanded[12]helicene) was the same as the corresponding [40]helicene, using a lower number of benzenes. In that way, impressive $|m|$ values can be obtained (up to 22.28×10^{-20} erg G^{-1} in expanded[50]helicene) only manipulating the geometry in a rational approach. As expected, the analysis of the densities and decomposition of the vector associated to the phenyl ring contributions (e.g. Figure S78) afforded essentially the same information as in the previous family, supporting, in a consistent way, that this kind of molecules present an intrinsic solenoid behavior in their excitation processes.

With these encouraging results in hand, we decided to prove whether the linear correlation between the inner area and $|m|$ was preserved in other helical structures. As a second case, we selected the *o*-OPE family, in which helical structures can be found in their fully folded conformations.[20,49–52] We optimized the geometry of helical *o*-OPEs ranging from one to ten loops (LC-ωPBE/6-31G*/PCM). In this family, each loop contains three phenylacetylene units, except for the smallest member, which contains an extra benzene ring. The nomenclature followed was n-*o*-OPE, where n stands for the number of phenyl rings. Thus, the family ranged from **4-*o*-OPE** (one loop) to **31-*o*-OPE** (ten loops). Using TD-DFT, we calculated ***m*** for the first 50 vertical electronic transitions. After performing the cluster analysis, a subgroup containing a unique transition vector aligned with the helix was again observed (see example of **10-*o*-OPE** in Figure 6 left). Conversely, for **4-*o*-OPE** and **7-*o*-OPE**, the family was composed of three transitions and two respectively, therefore, the maximum value was used in the correlation. A striking correlation ($R^2 = 0.9887$) was found by plotting $|m|$ against the inner area (Figure 7, blue squares). The decomposition analysis of ***m*** resulted in similar conclusions to the previous discussed case, the vector assigned to ***m*** appears due to a helical

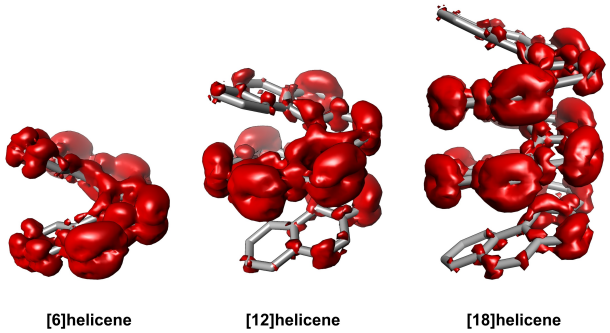

Figure 5. Magnetic dipole transition moment densities for the transition that represents a single independent subgroup in the cluster analysis displayed with an isosurface value of 0.005 a.u. in **[6]**, **[12]** and **[18]helicene**.

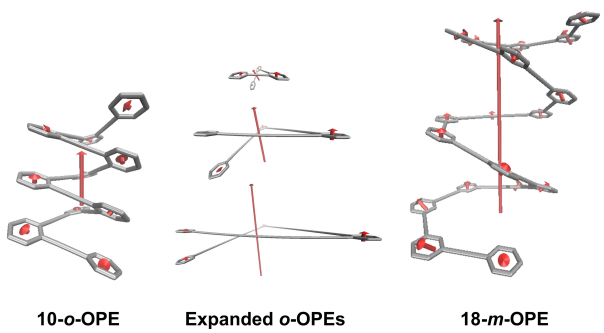

Figure 6. Optimized structures (LC-ωPBE/6-31G*/PCM) of selected examples of OPEs: **10-*o*-OPE, expanded *o*-OPEs** and **18-*m*-OPE** and orientation of the magnetic dipole transition moment (m) that represents an independent subgroup in the cluster analysis.

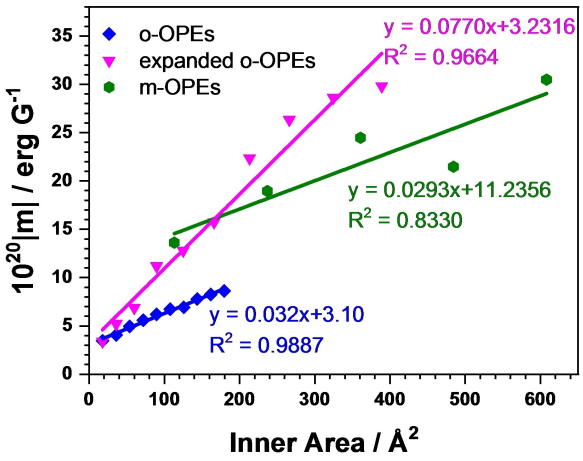

Figure 7. Correlation chart between the inner area and the calculated magnetic dipole transition moment module ($|m|$) for ***o*-OPEs** (blue squares)**, expanded *o*-OPEs** (pink triangles) and ***m*-OPEs** (green hexagons).

movement of electrons during the transition. Intriguingly, the magnitude of ***m*** was weaker for *o*-OPEs family, compared to helicenes and expanded helicenes with the same inner area. Thus, we hypothesized that the degree of conjugation has an effect in the correlation slope. Consequently, the enclosed area is not the only relevant feature to control in the design of compounds with impressive chiroptical properties.

At this point, we wondered whether such weaker $|m|$ is general. Therefore, we studied the trend using only one loop in which the encircled area was monotonically increased. Analogously to the family of [n]helicenes, we created an expanded *o*-OPE family increasing up to ten the number of alkynes connecting the phenyl rings (Figure 6, middle). A similar clustering analysis showed families composed by single or a couple of transitions in which representation of the most intense against the encircled area revealed again the expected correlation (Figure 7, pink triangles), at least for the first nine members of the series. A closer inspection of the final anomaly showed that during the minimization process the phenyl rings at the ends were rotated with respect to the inner phenyl ring and therefore the conjugation was interrupted. For a better understanding of the phenomenon, we artificially rotated the extrema to preserve the full conjugation. As a result, we recovered, in this later case, a better correlation. As in previous families, the magnetic dipole transition moment densities together with the decomposition of the dipole transition moment of single independent subgroups were analyzed (see SI, e.g., S111), showing an intense component in the helix axis.

To exhaustively evaluate this family and bearing in mind all the precedents, the ideal molecular arrangements are the ones magnifying the inner area for the same number of carbon atoms. Considering that *m*-OPEs are also able to generate helical structures, they are appealing candidates to be studied. It is worth noting that a single loop in a *m*-OPE represents about six single *o*-OPE loops in terms of inner area (113.27 vs 107.86 Å^2). Thus, we modelled *m*-OPEs with up to five loops (Figure 6, right), an equivalent area to **103-*o*-OPE**. Consistently, the correlation was found as expected (Figure 7, green hexagons, see ESI for more details). In fact, the most striking result is that the slope is similar to the one obtained for the *o*-OPE family (0.029 vs 0.032, respectively), thus perfectly fitting the expected values: a *m*-OPE loop is the equivalent of seven *o*-OPEs loops, owing to its area relationship. Considering an identical number of loops for *m*- and *o*-OPEs, a magnified ***m*** is obtained, clearly pointing out that the area is the critical factor and confirming our initial assumption.

The classic magnetic dipole moment formula refers to a closed loop of current where the relationship between the magnitude of ***m*** and the area would be perfect (Figure 1). Recently, Morasaki's group has described an analogue to a molecular loop in a chiral form with impressive chiroptical responses.[27] If our working hypothesis is right, the relationship between $|m|$ and the inner area must fit perfectly also for these systems. Therefore, as third case we created a set of five molecular circuits based on Morasaki's systems (Figure 8) and evaluated whether the aforementioned correlation exists. The results nicely fit the expectations with a linear dependence and alignment of the vector, being perpendicular to the π-conjugated system (Figure 9). Despite the correlation might resemble to reach a plateau, this can be attributed to the higher conformational flexibility of **chiral circuit 5** (Figure S153), which affects the estimation of its inner area and magnetic dipole transition moment This negative conformational effect must be considered in the design of synthetic objectives. In any case, the predicted $|m|$ values were enormous, up to 47×10^{-20} erg G^{-1}. These results show the unlimited influence of the inner area in the modulation of $|m|$, obtaining linear responses in systems with areas as big as 1000 Å^2.

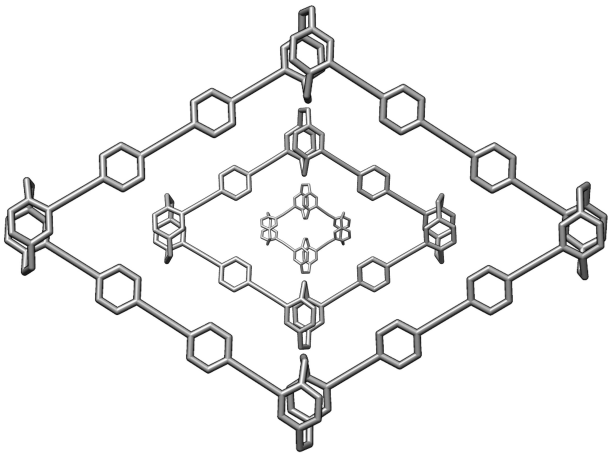

Figure 8. Optimized structures (LC-ωPBE/6-31G*/PCM) of **chiral circuits 1–3**.

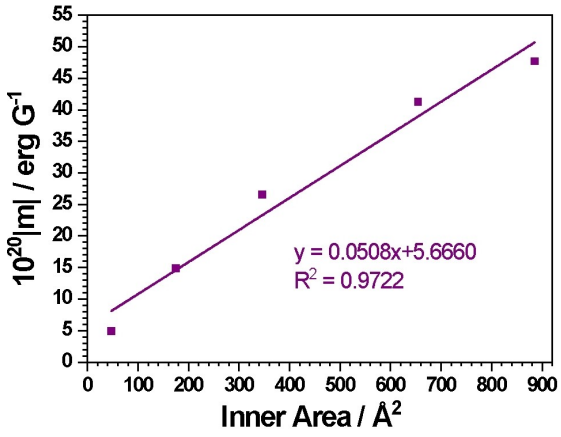

Figure 9. Correlation chart between the inner area and the calculated magnetic dipole transition moment module ($|m|$) for **chiral circuits**.

Conclusion

In this work we describe a remarkable linear relationship between the magnetic dipole transition moment and the inner area defined by chiral scaffolds in three different families of architectures (carbo[n]helicenes, *o*-OPEs and chiral molecular circuit based on paraphenylethynylene-linked paracyclophanes). The use of clustering methodologies has allowed an unsupervised classification of the transitions according to the value of this parameter. In most of the cases there is one group conformed by a single transition, which corresponds to the maximum value of $|m|$. Such m was observed to correlate with the inner area of the helical compounds under study (R^2 up to 0.9944), revealing the behavior of a molecular solenoid. Along these lines, increasing the inner area of the helix (enhancing the number of turns or the extension of the turn) permits to reach outstanding m values, leading to intense chiroptical responses. Considering the proposed relationship between the strength of chiroptical properties and spin filtering,[53] this correlation provides a tool for the future development of more efficient optoelectronic and spin-selective devices.

Supporting Information

The authors have cited additional references within the Supporting Information.[32–39,40,42,44,54–56]

Acknowledgements

Financial support is acknowledged: grant PID2020-113059GB-C21 funded by MCIN/AEI/10.13039/501100011033, grant PID2020-112754GB-I00 funded by MCIN/AEI/10.13039/501100011033, grant PID2022-137403NA-I00 funded by MCIN/AEI/10.13039/501100011033 and by "ERDF A way of making Europe". R.G.U. also acknowledges for his FPU contract (FPU 20/03582). C.M.C. thanks Junta de Andalucía for a post-doctoral grant (POSTDOC_21_00139). S. M. L. thanks Junta de Andalucía for a postdoctoral grant. We thank Centro de Servicio de Informática y Redes de Comunicaciones (CSIRC), Universidad de Granada, for providing the computing time. We thank Linda A. Zotti for her helpful comments and assistance. We also thank for the funding for open access charge to Universidad de Granada /CBUA.

Conflict of Interest

The authors declare no conflict of interest.

Data Availability Statement

The data that support the findings of this study are available in the supplementary material of this article.

Keywords: Chirality · Circular Dichroism · Clustering Method · Density Functional Calculations · Helical Structures

[1] X. Wang, S. Ma, B. Zhao, J. Deng, *Adv. Funct. Mater.* **2023**, *33*, 2214364.
[2] Y. Yang, R. C. da Costa, M. J. Fuchter, A. J. Campbell, *Nat. Photonics* **2013**, *7*, 634–638.
[3] J. Han, S. Guo, H. Lu, S. Liu, Q. Zhao, W. Huang, *Adv. Opt. Mater.* **2018**, *6*, 1800538.
[4] Y. Yang, N. Li, J. Miao, X. Cao, A. Ying, K. Pan, X. Lv, F. Ni, Z. Huang, S. Gong, C. Yang, *Angew. Chem. Int. Ed.* **2022**, *61*, e202202227.
[5] D.-W. Zhang, M. Li, C.-F. Chen, *Chem. Soc. Rev.* **2020**, *49*, 1331–1343.
[6] Y. Sang, J. Han, T. Zhao, P. Duan, M. Liu, *Adv. Mater.* **2020**, *32*, 1900110.
[7] A. H. G. David, R. Casares, J. M. Cuerva, A. G. Campaña, V. Blanco, *J. Am. Chem. Soc.* **2019**, *141*, 18064–18074.
[8] P. Reiné, A. M. Ortuño, S. Resa, L. Álvarez de Cienfuegos, V. Blanco, M. J. Ruedas-Rama, G. Mazzeo, S. Abbate, A. Lucotti, M. Tommasini, S. Guisán-Ceinos, M. Ribagorda, A. G. Campaña, A. Mota, G. Longhi, D. Miguel, J. M. Cuerva, *Chem. Commun.* **2018**, *54*, 13985–13988.
[9] M. Suarez, G. B. Schuster, *J. Am. Chem. Soc.* **1995**, *117*, 6732–6738.
[10] F. Evers, A. Aharony, N. Bar-Gill, O. Entin-Wohlman, P. Hedegård, O. Hod, P. Jelinek, G. Kamieniarz, M. Lemeshko, K. Michaeli, V. Mujica, R. Naaman, Y. Paltiel, S. Refaely-Abramson, O. Tal, J. Thijssen, M. Thoss, J. M. van Ruitenbeek, L. Venkataraman, D. H. Waldeck, B. Yan, L. Kronik, *Adv. Mater.* **2022**, *34*, 2106629.
[11] R. Naaman, Y. Paltiel, D. H. Waldeck, *Nat. Chem. Rev.* **2019**, *3*, 250–260.
[12] T. K. Das, F. Tassinari, R. Naaman, J. Fransson, *J. Phys. Chem. C* **2022**, *126*, 3257–3264.
[13] T. S. Metzger, H. Batchu, A. Kumar, D. A. Fedotov, N. Goren, D. K. Bhowmick, I. Shioukhi, S. Yochelis, I. Schapiro, R. Naaman, O. Gidron, Y. Paltiel, *J. Am. Chem. Soc.* **2023**, *145*, 3972–3977.
[14] K. Michaeli, N. Kantor-Uriel, R. Naaman, D. H. Waldeck, *Chem. Soc. Rev.* **2016**, *45*, 6478–6487.
[15] Z. Xie, T. Z. Markus, S. R. Cohen, Z. Vager, R. Gutierrez, R. Naaman, *Nano Lett.* **2011**, *11*, 4652–4655.

[16] B. Göhler, V. Hamelbeck, T. Z. Markus, M. Kettner, G. F. Hanne, Z. Vager, R. Naaman, H. Zacharias, *Science* **2011**, *331*, 894–897.
[17] Y. Nagata, T. Mori, *Front. Chem.* **2020**, *8*, 448.
[18] G. Mazzeo, S. Ghidinelli, R. Ruzziconi, M. Grandi, S. Abbate, G. Longhi, *ChemPhotoChem* **2022**, *6*, e202100222.
[19] I. Tinoco, R. W. Woody, *J. Chem. Phys.* **1964**, *40*, 160–165.
[20] A. M. Ortuño, P. Reiné, S. Resa, L. Álvarez de Cienfuegos, V. Blanco, J. M. Paredes, A. J. Mota, G. Mazzeo, S. Abbate, J. M. Ugalde, V. Mujica, G. Longhi, D. Miguel, J. M. Cuerva, *Org. Chem. Front.* **2021**, *8*, 5071–5086.
[21] K. Fujise, E. Tsurumaki, G. Fukuhara, N. Hara, Y. Imai, S. Toyota, *Chem. Asian J.* **2020**, *15*, 2456–2461.
[22] G. Huo, T. M. Fukunaga, X. Hou, Y. Han, W. Fan, S. Wu, H. Isobe, J. Wu, *Angew. Chem. Int. Ed.* **2023**, *62*, e202218090.
[23] Y. Nakakuki, T. Hirose, K. Matsuda, *J. Am. Chem. Soc.* **2018**, *140*, 15461–15469.
[24] G. R. Kiel, H. M. Bergman, A. E. Samkian, N. J. Schuster, R. C. Handford, A. J. Rothenberger, R. Gomez-Bombarelli, C. Nuckolls, T. Don Tilley, *J. Am. Chem. Soc.* **2022**, *144*, 23421–23427.
[25] Y. Shen, N. Yao, L. Diao, Y. Yang, X. Chen, H. Gong, *Angew. Chem. Int. Ed.* **2023**, *135*, e202300840.
[26] M. Toya, T. Omine, F. Ishiwari, A. Saeki, H. Ito, K. Itami, *J. Am. Chem. Soc.* **2023**, *145*, 11553–11565.
[27] A. Morisaki, R. Inoue, Y. Morisaki, *Chem. Eur. J.* **2023**, *29*, e202203533.
[28] K. Drab, M. Daszykowski, *J. AOAC Int.* **2014**, *97*, 29–38.
[29] G. Marton, M. A. J. Koenis, H. Liu, C. A. Bewley, W. J. Buma, V. P. Nicu, *Angew. Chem. Int. Ed.* **2023**, *62*, e202307053.
[30] G. James, D. Witten, T. Hastie, R. Tibshirani, *An Introduction of Statistical Learning*, Springer, Berlin, **2021**, pp. 497–552.
[31] N. Altman, M. Krzywinski, *Nat. Methods* **2017**, *14*, 545–546.
[32] M. J. Frisch, G. W. Trucks, H. B. Schlegel, G. E. Scuseria, M. A. Robb, J. R. Cheeseman, G. Scalmani, V. Barone, B. Mennucci, G. A. Petersson, H. Nakatsuji, M. Caricato, X. Li, H. P. Hratchian, A. F. Izmaylov, J. Bloino, G. Zheng, J. L. Sonnenberg, M. Hada, M. Ehara, K. Toyota, R. Fukuda, J. Hasegawa, M. Ishida, T. Nakajima, Y. Honda, O. Kitao, H. Nakai, T. Vreven, J. A. Montgomery Jr, J. E. Peralta, F. Ogliaro, M. Bearpark, J. J. Heyd, E. Brothers, K. N. Kudin, V. N. Staroverov, R. Kobayashi, J. Normand, K. Raghavachari, A. Rendell, J. C. Burant, S. S. Iyengar, J. Tomasi, M. Cossi, N. Rega, J. M. Millam, M. Klene, J. E. Knox, J. B. Cross, V. Bakken, C. Adamo, J. Jaramillo, R. Gomperts, R. E. Stratmann, O. Yazyev, A. J. Austin, R. Cammi, C. Pomelli, J. W. Ochterski, R. L. Martin, K. Morokuma, V. G. Zakrzewski, G. A. Voth, P. Salvador, J. J. Dannenberg, S. Dapprich, A. D. Daniels, O. Farkas, J. B. Foresman, J. V. Ortiz, J. Cioslowski, D. J. Fox, Gaussian09. Revission B.01, **2010**.
[33] O. A. Vydrov, G. E. Scuseria, *J. Chem. Phys.* **2006**, *125*, 234109.
[34] M. M. Francl, W. J. Pietro, W. J. Hehre, J. S. Binkley, M. S. Gordon, D. J. DeFrees, J. A. Pople, *J. Chem. Phys.* **1982**, *77*, 3654–3665.
[35] S. Miertuš, E. Scrocco, J. Tomasi, *Chem. Phys.* **1981**, *55*, 117–129.
[36] A. D. Becke, *J. Chem. Phys.* **1993**, *98*, 5648–5652.
[37] C. Lee, W. Yang, R. G. Parr, *Phys. Rev. B* **1988**, *37*, 785–789.
[38] P. J. Stephens, F. J. Devlin, C. F. Chabalowski, M. J. Frisch, *J. Phys. Chem.* **1994**, *98*, 11623–11627.
[39] Y. Zhao, D. G. Truhlar, *Theor. Chem. Acc.* **2008**, *120*, 215–241.
[40] C. El-Morr, M. Jammal, H. Ali-Hassan, W. El-Hallak, *Machine Learning for Practical Decision Making*, Springer, Berlin, **2022**, pp. 361–384.
[41] V. Satopaa, J. Albrecht, D. Irwin, B. Raghavan, in *2011 31st International Conference on Distributed Computing Systems Workshops*, IEEE, **2011**, pp. 166–171.
[42] F. Pedregosa, G. Varoquaux, A. Gramfort, V. Michel, B. Thirion, O. Grisel, M. Blondel, A. Müller, J. Nothman, G. Louppe, P. Prettenhofer, R. Weiss, V. Dubourg, J. Vanderplas, A. Passos, D. Cournapeau, M. Brucher, M. Perrot, É. Duchesnay, *J. Mach. Learn. Res.* **2011**, *12*, 2825–2830.
[43] P. Ravat, *Chem. Eur. J.* **2021**, *27*, 3957–3967.
[44] T. Lu, F. Chen, *J. Comput. Chem.* **2012**, *33*, 580–592.
[45] H.-C. Huang, Y.-C. Hsieh, P.-L. Lee, C.-C. Lin, Y.-S. Ho, W.-K. Shao, C.-T. Hsieh, M.-J. Cheng, Y.-T. Wu, *J. Am. Chem. Soc.* **2023**, *145*, 10304–10313.
[46] J. Tan, X. Xu, J. Liu, S. Vasylevskyi, Z. Lin, R. Kabe, Y. Zou, K. Müllen, A. Narita, Y. Hu, *Angew. Chem. Int. Ed.* **2023**, *62*, e202218494.
[47] K. Kato, Y. Segawa, K. Itami, *Synlett* **2019**, *30*, 370–377.
[48] S. H. Pun, K. M. Cheung, D. Yang, H. Chen, Y. Wang, S. V. Kershaw, Q. Miao, *Angew. Chem. Int. Ed.* **2022**, *134*, e202113203.
[49] S. Resa, P. Reiné, L. Álvarez de Cienfuegos, S. Guisán-Ceinos, M. Ribagorda, G. Longhi, G. Mazzeo, S. Abbate, A. J. Mota, D. Miguel, J. M. Cuerva, *Org. Biomol. Chem.* **2019**, *17*, 8425–8434.
[50] S. Resa, D. Miguel, S. Guisán-Ceinos, G. Mazzeo, D. Choquesillo-Lazarte, S. Abbate, L. Crovetto, D. J. Cárdenas, M. C. Carreño, M. Ribagorda, G. Longhi, A. J. Mota, L. Álvarez de Cienfuegos, J. M. Cuerva, *Chem. Eur. J.* **2018**, *24*, 2653–2662.
[51] J. C. Nelson, J. G. Saven, J. S. Moore, P. G. Wolynes, *Science* **1997**, *277*, 1793–1796.
[52] M. S. Gin, T. Yokozawa, R. B. Prince, J. S. Moore, *J. Am. Chem. Soc.* **1999**, *121*, 2643–2644.
[53] B. P. Bloom, B. M. Graff, S. Ghosh, D. N. Beratan, D. H. Waldeck, *J. Am. Chem. Soc.* **2017**, *139*, 9038–9043.
[54] E. F. Pettersen, T. D. Goddard, C. C. Huang, G. S. Couch, D. M. Greenblatt, E. C. Meng, T. E. Ferrin, *J. Comput. Chem.* **2004**, *25*, 1605–1612.
[55] "Chemcraft, Graphical software for visualization of quantum chemistry computations. https://www.chemcraftprog.com".
[56] W. Humphrey, A. Dalke, K. Schulten, *J. Mol. Graphics* **1996**, *14*, 33–38.

Manuscript received: November 3, 2023
Accepted manuscript online: December 5, 2023
Version of record online: December 20, 2023